Int. J. Electrochem. Sci., 7 **(2012)** 376 - 386

International Journal of
ELECTROCHEMICAL
SCIENCE
www.electrochemsci.org

Effect of Silicon Porosity on Solar Cell Efficiency

Khaldun A. Salman[*], *Z. Hassan, Khalid Omar*

Nano-Optoelectronics Research and Technology Laboratory, School of Physics, University Sains Malaysia, Penang 11800, Malaysia
[*]E-mail: khaldunphysics@gmail.com

Received: 10 November 2011 / *Accepted:* 4 December 2011 / *Published:* 1 January 2012

Porous silicon (PS) layers were fabricated on n-type crystalline silicon (c-Si) wafers of (100) and (111) orientations using photoelectrochemical etching (PECE) process at etching time of 20 min, current density of 60 mA/cm^2, and fixed electrolyte solution HF:C_2H_5OH (1:4). Moreover, PS layers fabricated on p-type c-Si wafers of (100) and (111) orientations using electrochemical etching (ECE) process were prepared under similar parameters. Nanopores with an average diameter of 5.7 nm were formed in the n-PS (100) layer. These nanopores increased the porosity of the material to 91% compared with those of the samples with different orientation and Si type. A greater blue shift luminescence was observed in the n-PS (100) layer compared with those of the other samples. The lowest effective reflectance was obtained with the n-PS (100) layer that exhibited excellent light-trapping at wavelengths ranging from 400 to 1000 nm. Solar cells were fabricated based on the PS anti-reflection coating (ARC) layers. The current-voltage characteristics of the solar cells were examined under 100 mW/cm^2 illumination. A highly efficient (15.5%) solar cell was obtained with n-PS (100) ARC layer compared with those solar cells with other layer types. In the present paper, the effect of the porosity of the PS ARC layers on the solar cell efficiency based on the n- and p-type regions with (100) and (111) orientations was investigated.

Keywords: Porosity; Electrochemical etching; Porous silicon; Anti-reflection coating; Solar cell.

1. INTRODUCTION

Porous silicon (PS), a nanostructured material, has attracted considerable attention as a measure to enhance the optical properties of silicon (Si). The formation of PS layers on crystalline Si (c-Si) wafers using electrochemical etching (ECE) exhibits photoluminescent and electroluminescent properties similar to those of semiconductors with direct energy gap [1]. PS has emerged as an attractive material in the field of electronics and optoelectronics due to its broad band gap, wide optical transmission range (700–1000 nm), wide absorption spectrum, surface roughening, and good anti-reflection coating (ARC) [2]. The surface roughness and lower effective refractive index, which can

reduce the reflection losses of sunlight radiation, are the primary factors that enhance PS compared with c-Si [3].

In the visible (VIS) region, the refractive index decreases with increasing porosity, in contrast to the increasing edge absorption coefficient with an increase in porosity [4]. The porosity of the PS layer increases with increasing current density and decreasing HF concentrations. This condition is also controlled by substrate doping [5]. Thus, a highly porous PS layer can enhance the efficiency of solar cells by increasing light trapping into the active region [6]. This layer can also be used as ARC to serve as gutter centers and reduce the impurity levels of the Si substrate [7]. Moreover, a highly porous PS layer further increases the efficiency and absorbs more light energy in c-Si solar cells [8].

A highly porous PS layer is essential for high photoluminescence (PL) efficiency and in the acquisition of highly efficient solar cells. An inefficient luminescence results from an inhomogeneous material of low porosity [9].The observed visible luminescence from the PS layer is caused by the increasing energy band gap of the PS layer compared with bulk Si [10]. Several samples of PS monolayers and multilayers were prepared under different anodization conditions with fixed hydrofluoric (HF) concentration and current density. The photovoltaic effect of these structures has been reported [11, 12].

In the present study, photoelectrochemical etching (PECE) and ECE processes were used to fabricate PS layers on the n- and p-type regions with (100) and (111) orientations using an etching time of 20 min, current density of 60 mA/cm^2, and fixed electrolyte solution $HF:C_2H_5OH$ (1:4). The morphologies and optical properties of the PS layers were also examined. The objective of the present study was to fabricate highly efficient solar cell using highly porous PS layer as ARC.

2. EXPERIMENTAL

N- and p-type float-zone (FZ) c-Si wafers (resistivity, 1 Ωcm; thickness, 300 μm; and orientation, (100) and (111)) were used as substrates. Before the etching process, the substrates were cleaned to remove the oxide layer using the Radio Corporation of America method. Then, the c-Si samples were dipped in a solution of $HF:H_2O$ (1:50) at 25 °C to remove the native oxide and some ionic contaminants.

PS layers were fabricated by PECE process for n-type c-Si wafer and by ECE for p-type c-Si wafer with a 0.57 cm radius similar to the size of the opened-circular of the Teflon cell. Teflon was used to fabricate the ECE cell that had a circular aperture at the bottom that is sealed with c-Si samples. The cell was a two-electrode system connected to the c-Si samples as the anode and platinum (Pt) as the cathode. The cell was called PECE if the illumination was positioned over the n-type c-Si samples for maximum possible illumination and to generate the required holes for dissolution [5]. In contrast, the cell is called ECE if the p-type c-Si samples were not illuminated, (Fig. 1).

The c-Si samples were placed in an electrolyte solution HF (48%):C_2H_5OH (98%) (1:4, by volume) to enable the conduction of electrons inside the solution. A current density of 60 mA/cm^2 and an etching time of 20 min were used to prepare the PS layers on the front side of the c-Si samples.

Synthesis was performed at RT. The samples were rinsed in ethanol and dried in air after the etching process.

The prepared samples of PS layers with different porosities were used to fabricate solar cells using the following procedure. The samples were coated with photoresist, and then a mask was placed directly above the PS layers. The samples were exposed to UV radiation for 40 s for the formation of a patterned coating. N- and p-type doping was achieved using the spin coating method by placing phosphorus and boron liquid at the center of the PS layers, followed by spin coating at RT at 1000 rpm for 10 s. Then, the PS layers were placed in a furnace at 100 °C for 15 min to remove moisture. Dopant was diffused using a tube furnace at 1000 °C for 60 min under flowing (4 Lmin $^{-1}$) nitrogen gas.

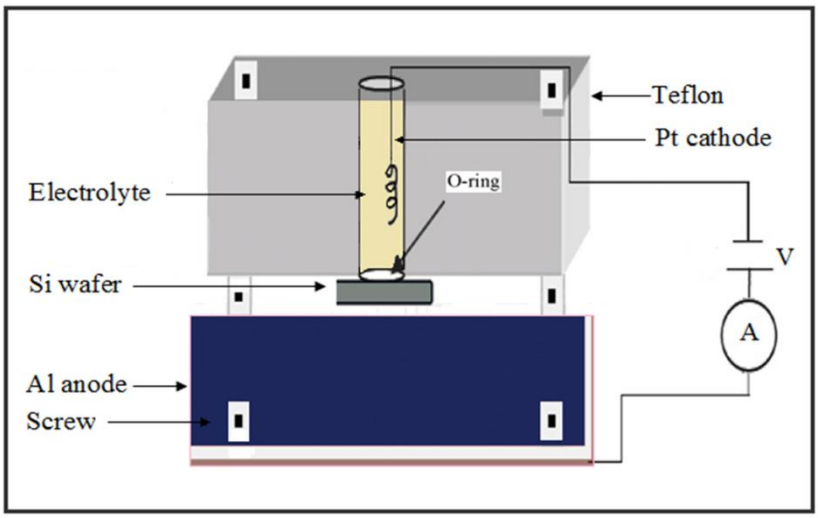

Figure 1. Schematic ECE cell set-up.

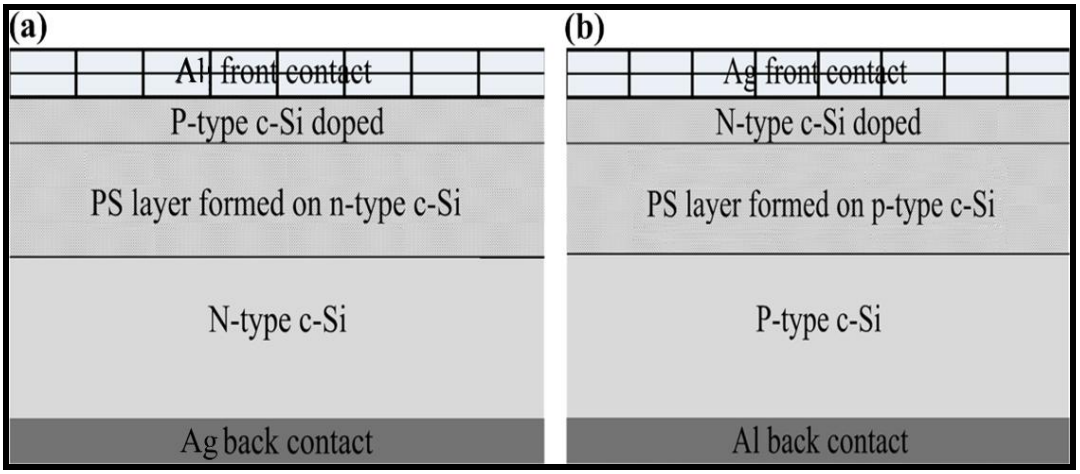

Figure 2(a, b). Schematic illustrations of solar cells with PS layers formed on n-type c-Si (100) and (111) orientations and with PS layers formed on n-type c-Si (100) and (111) orientations, respectively.

Silver evaporation was used on the front (n-type) side of the samples to form a metallization grid pattern, whereas aluminum evaporation was used on the back (p-type) side to form a reflector contact. Annealing was achieved at 400 °C for 20 min to ensure optimal contact.

Fig. 2(a, b) shows the schematic illustrations of the solar cells with PS layers formed on n-type c-Si (100) and (111) orientations and with PS layers formed on n-type c-Si (100) and (111) orientations, respectively.

In the case of the n-type substrate, the p-n junction placed in the front side and the solar cell was the front junction solar cell. However, the front side will be the p-type, and the back side will be the n-type, as shown in Fig. 2(a).

Then in the case of the p-type substrate, the p-n junction was also placed in the front side, and the solar cell was the front junction solar cell. Here, the front side will be the n-type, and the back side will be the p-type, as shown in Fig. 2(b).

In addition, in the size of the fabricated solar cells was 1 cm^2 and the p-n junction was placed in the porous layers.

Scanning electron microscopy (SEM) analyses (JSM-6460 LV, Japan) were used to determine the surface morphology of the PS layers. PL studies were performed for all PS layers using a spectroscopy system (Jobin Yvon HR 800 UV, Edison, NJ, USA). The optical reflectance of the c-Si sample and PS layers were obtained using an optical reflectometer (Filmetrics, F20, USA). Current-voltage (I-V) characteristics were studied under air mass 1.5 global (AM 1.5G) illumination [13].

3. RESULTS AND DISCUSSIONS

PS layers were fabricated on the n- and p-type c-Si wafers with (100) and (111) orientations at 20 min etching time with fixed HF concentration and current density.

Fig. 3(a) shows an SEM image of the PS layer formed on the n-type c-Si (100) sample, in which randomly distributed pores are observed on the surface of the layer. Several pores had star-like appearance and elongated shapes.

The surface of the c-Si sample was completely etched and consisted of numerous tiny pores formed over the soft wall. The formation of numerous new tiny pores inside the initial pores can be distinguished clearly. Additionally, highly dense pores were evident. The high porosity of approximately 91% was calculated using Eq. (1) [14],

$$P\ (\%) = \frac{m_1 - m_2}{m_1 - m_3}, \qquad (1)$$

where m_1 is the sample weight before anodization, m_2 is the sample weight after anodization, and m_3 is the sample weight after removing the PS layer with 3% KOH solution for 50 s [6].

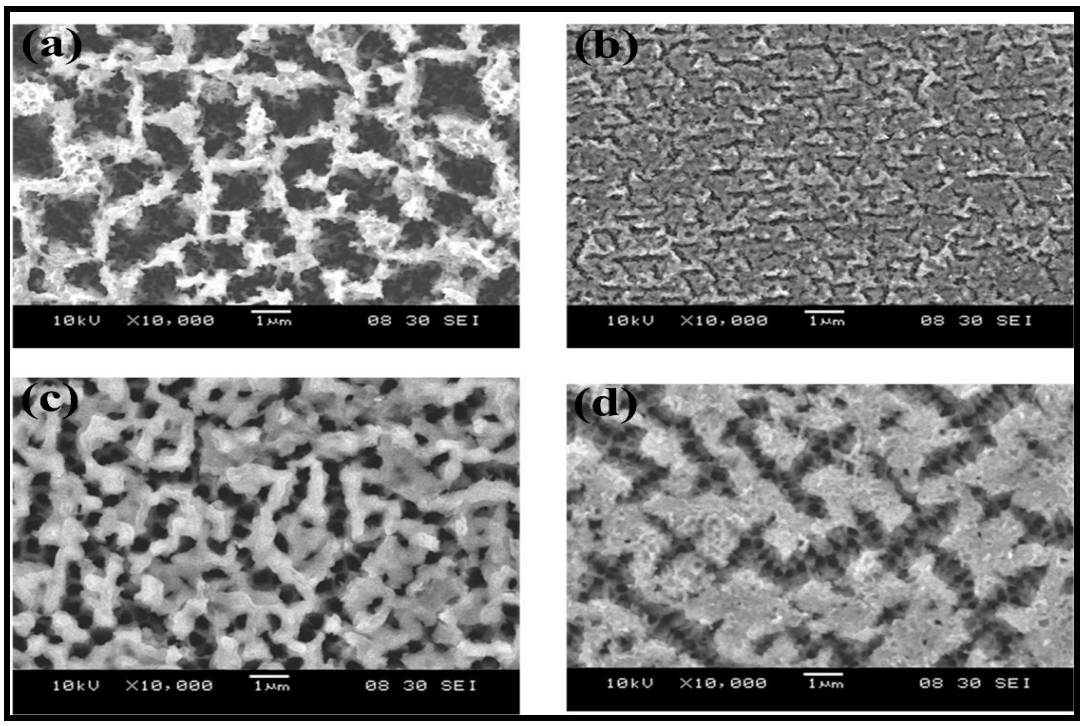

Figure 3. SEM images of PS layers formed on (a) n-type c-Si (100), (b) n-type c-Si (111), (c) p-type c-Si (100), and (d) p-type c-Si (111) samples.

Fig. 3(b) illustrates the SEM image of the PS layer formed on the n-type c-Si (111) sample. The surface of the c-Si sample cracked, and pores were not evidently observed. The etched surface became rougher than the c-Si surface, indicating low porosity (approximately 14.5%).

Fig. 3(c) demonstrates the SEM image of the PS layer formed on the p-type c-Si (100) sample. Pores with sphere-like appearances and thick walls were evidently randomly distributed on the PS surface. A modest density of pores was observed, and porosity was approximately 45%, higher than the 27% porosity of the PS layer formed on the p-type c-Si (111) sample (Fig. 3(d)). The surface of the c-Si sample cracked, and numerous new pores evidently formed inside the cracks. Additionally, the surface of the c-Si sample was completely etched and consisted of numerous discrete pores that formed over the wall that did not crack, and the pore walls widened, reducing the number of pores on the PS surface. Hence, porosity decreased.

The average pore diameter (d) for the PS layer formed on the n-type c-Si (100) wafers was 5.7 nm and calculated using Eq. (2) [15],

$$E(eV) = E_g + \frac{h^2}{8d^2}\left[\frac{1}{m_e^*} + \frac{1}{m_h^*}\right], \quad (2)$$

where E (eV) is the energy band gap of the PS layer calculated from the PL peak, E_g is the energy band gap of bulk c-Si, h is Planck's constant=4.13×10^{-15} eV·s, whereas m_e^* and m_h^* are the

electron and hole effective masses, respectively (at 300 K, $m_e^*=0.19m_o$, $m_h^*=0.16m_o$, and $m_o=9.109x10^{-31}$ kg).

The use of a pore size with an average diameter of 5.7 nm in the n-PS (100) layer led to an increase in porosity to 91% and the presence of a remarkable blue shift in the maximum PL intensity and the lowest effective reflectance as will discuss later. Therefore, the refractive index decreased with respect to high porosity, resulting in an increase in the short-circuit current (I_{sc}) and open-circuit voltage (V_{oc}) of up to 33.90 mA/cm^2 and 595.00 mV, respectively." These increases in turn led to an enhanced conversion efficiency of 15.50% as mentioned in Table 1.

Fig. 4 shows SEM cross-sectional images of PS layers formed on n- and p-types with (100) and (111) orientations. The thickness of PS layers increased with increasing porosity. The thickest layer was approximately 62.50 μm for the n-type c-Si (100) sample.

The PS layers were easily distinguished due to the different structures between the PS layers and c-Si substrates. The formation of PS layers was not uniform due to the inhomogeneous formation of pores on the PS surfaces. The irregular distribution of the pores could enhance the photo conversion as a result of the widened PL peaks.

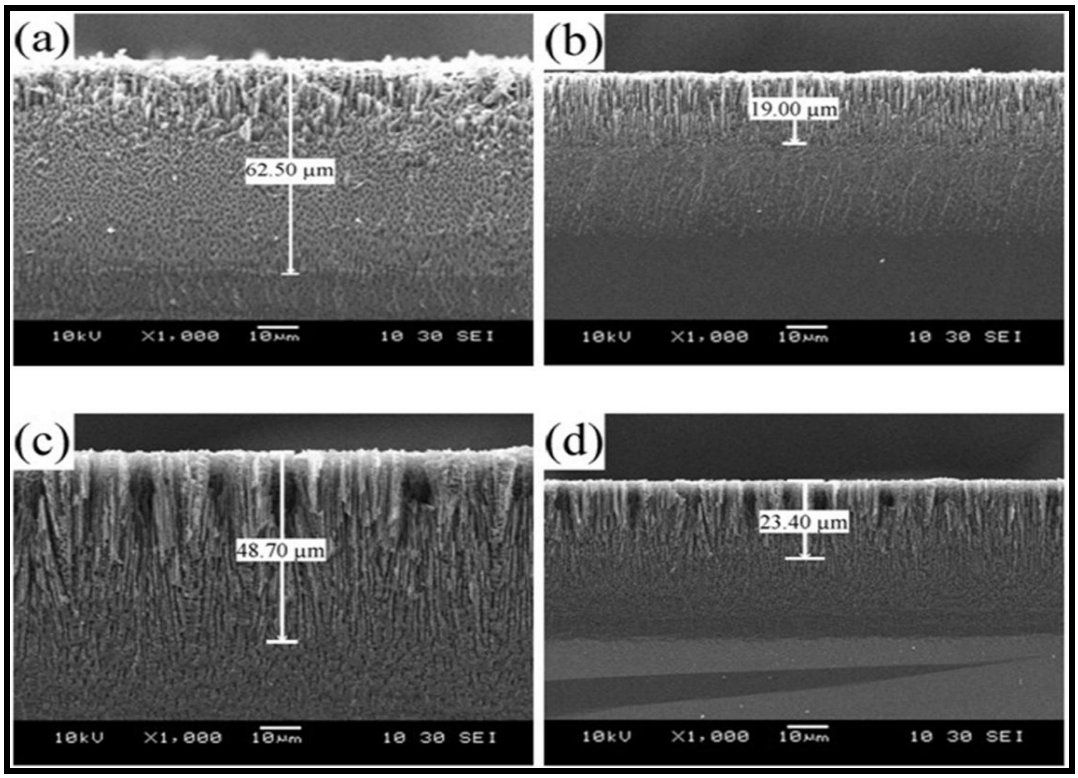

Figure 4. SEM cross-sectional images of the PS layers formed on (a) n-type c-Si (100), (b) n-type c-Si (111), (c) p-type c-Si (100), and (d) p-type c-Si (111) samples.

Fig. 5 shows the PL spectra of PS layers formed on n- and p-type regions with (100) and (111) orientations using He-Cd laser (λ=325 nm) at RT. The PL intensity of the PS layers increases with increasing porosity. Consequently, a thicker PS layer formed on the c-Si n-type (100) compared with

those of the other samples. The maximum PL intensity of the PS layer formed on the n-type c-Si (100) has been observed at 639 nm (1.940 eV) with a full-width and half maximum of approximately 145 nm as a result of the high porosity and completely etched PS layer of this sample. This phenomenon indicates that PL intensity is proportional to the number of emitted photons on the PS surface. Therefore, according to the PL measurements, the n-type c-Si (100) is the optimum c-Si type and orientation to prepare the PS layer. This condition is attributed to the increasing total volume of nanocrystallites on the PS surface according to the increasing PL intensity [16].

PL results show that the energy band gap increased from 1.12 eV for the c-Si sample to 1.940 eV for the PS layer formed on the n-type c-Si (100). This result indicates a remarkable blue shift of the maximum PL intensity. The particles are confined in a lower dimension according to quantum confinement effects [17,18]. Hence, the probability of the recombination of the electrons and holes is low in a low dimensional structure, resulting in high efficiency and high energy.

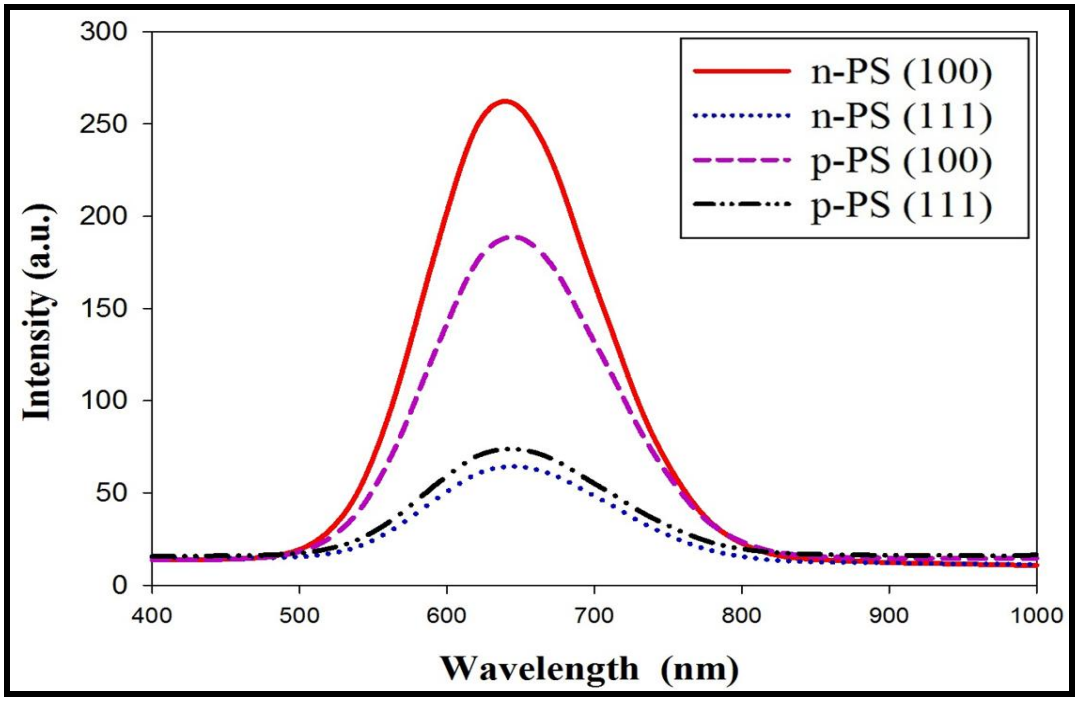

Figure 5. PL spectra of PS layers formed on the n- and p-type regions with (100) and (111) orientations.

Fig. 6 shows the reflection spectra of the PS layers on the n- and p-type regions with (100) and (111) orientations compared with the c-Si sample. The lowest effective reflectance was obtained from the PS layer formed on the n-type c-Si (100) sample, which evidently reduced light reflection and increased light-trapping at wavelengths from 400 to 1000 nm, compared with reflectivities of the other samples. The PS layer consisted of nano-Si crystals and nanopores. Therefore, the refractive index decreased and was controlled by the pores with respect to high porosity, resulting in a decreased reflection [19].

The maximum reduction in light reflection ranged from 450 to 650 nm. A slight increase in reflection occurred from 650 to 1000 nm, probably due to the random distribution of the pores and increased roughness of the PS surface. The attenuation of reflectivity was caused by the light transmission at the porous and bulk interface [20]. The PS ARC layer in the solar cells is a very important parameter to enhance photoconversion and increase light absorption in the VIS region of the solar spectrum, which is expected to increase the efficiency of solar cells.

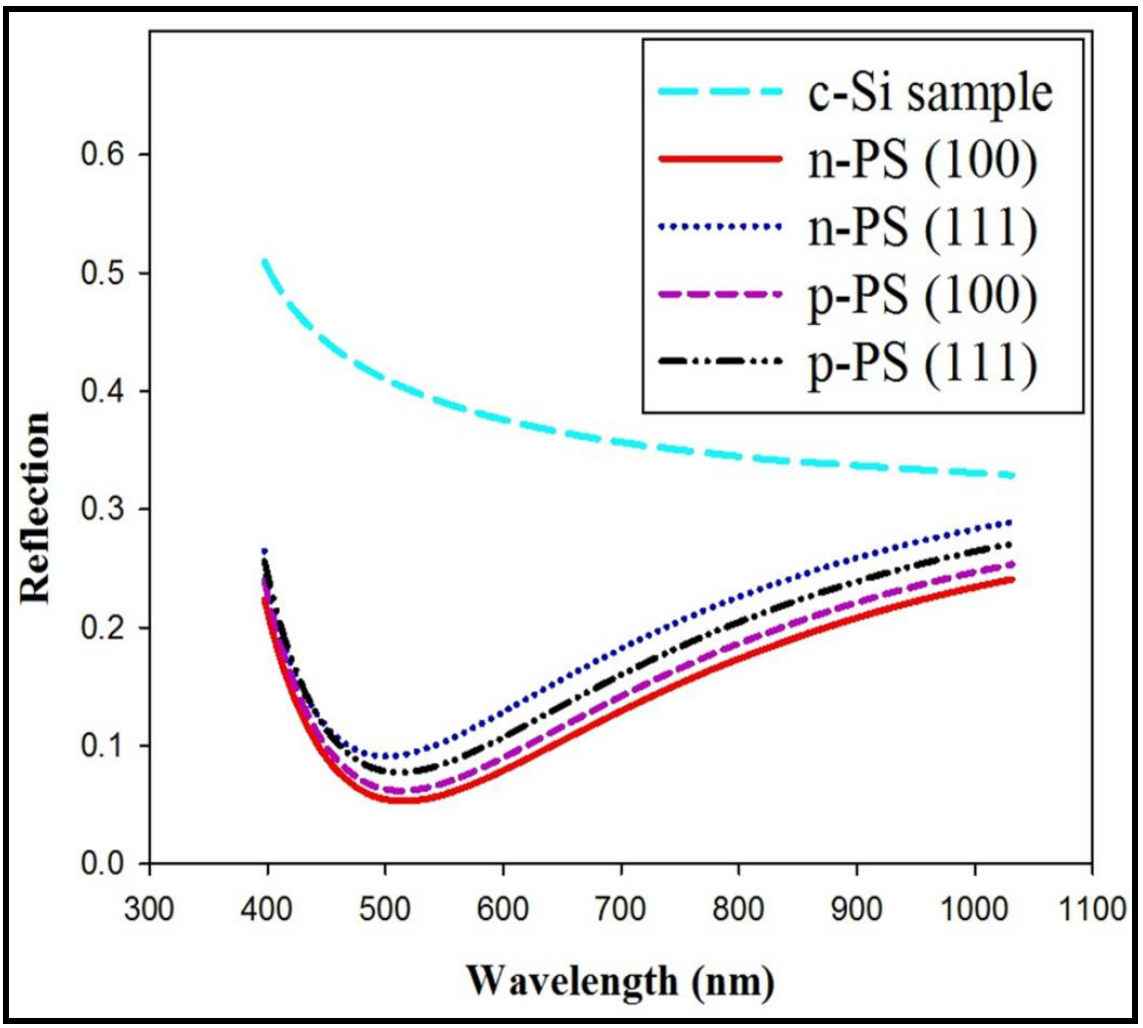

Figure 6. Reflection spectra of PS layers formed on the n- and p-type regions with (100) and (111) orientations compared with the c-Si sample.

Fig. 7 shows the increase in the efficiency of the solar cell with the PS ARC layer based on n-type c-Si (100) sample compared with the efficiency of the solar cells based on the PS ARC formed on the n-type c-Si (100), n-type c-Si (111), p-type c-Si (100), and p-type c-Si (111) samples, including the solar cell without PS ARC layer. The solar cells were characterized under 100 mW/cm^2 illumination.

The results show that the solar cell with the PS ARC layer based on n-type c-Si (100) displays an increased short-circuit current (I_{sc}) and open-circuit voltage (V_{oc}) up to 33.90 mA/cm^2 and 595.00 mV, respectively, leading to an increased conversion efficiency of 15.50% (Table 1).

Compared with other solar cells with the PS ARC formed on the n-type c-Si (111), p-type c-Si (100), and p-type c-Si (111) samples, these cells were found to have an I_{sc} of 20.50, 29.05, and 27.15 mA/cm^2, respectively, and a V_{oc} of 500, 545, and 510 mV, respectively. The efficiency values were 7.20%, 12.35%, and 9.70 %, respectively.

Therefore, the efficient solar cell was that which used the n-PS (100) ARC layer, p-PS (100) ARC layer, p-PS (111) ARC layer, and n-PS (111) ARC layer, in this order of efficiency.

The PS ARC layer based on the n-type c-Si (100) enhanced and increased the light conversion efficiency of the solar cell through the trapping of the incident radiation. This phenomenon is caused by the heterogeneous properties of the PS ARC layer, leading to increased I_{sc} and V_{oc}. These values were used with other values of maximum voltage (I_m) and maximum current (V_m) to calculate the conversion efficiency of the c-Si solar cell as follows [Eq. (3)]:

Table 1. I-**V** measurements of solar cells based on the PS layers formed on the n- and p-type regions with (100) and (111) orientations compared with the solar cell without a PS layer.

Solar cells	V_m (mV)	J_m (mA/cm^2)	V_{oc} (mV)	J_{sc} (mA/cm^2)	FF %	η %
Without PS layer	287.90	12.67	367.20	14.46	68.65	3.64
With PS layer formed on n-type c-Si (100)	503.00	30.82	595.00	33.90	76.40	15.50
With PS layer formed on n-type c-Si (111)	400.00	18.00	500.00	20.50	70.24	7.20
With PS layer formed on p-type c-Si (100)	455.00	27.15	545.00	29.05	78.02	12.35
With PS layer formed on p-type c-Si (111)	435.00	22.30	510.00	27.15	70.00	9.70

$$\eta = \frac{P_m}{P_{in}} = \frac{I_m V_m}{P_{in}}, \quad (3)$$

where P_m and P_{in} are the output and incident powers, respectively.
The fill factor (FF) was calculated by Eq. (4),

$$FF = \frac{I_m V_m}{I_{sc} V_{oc}}. \quad (4)$$

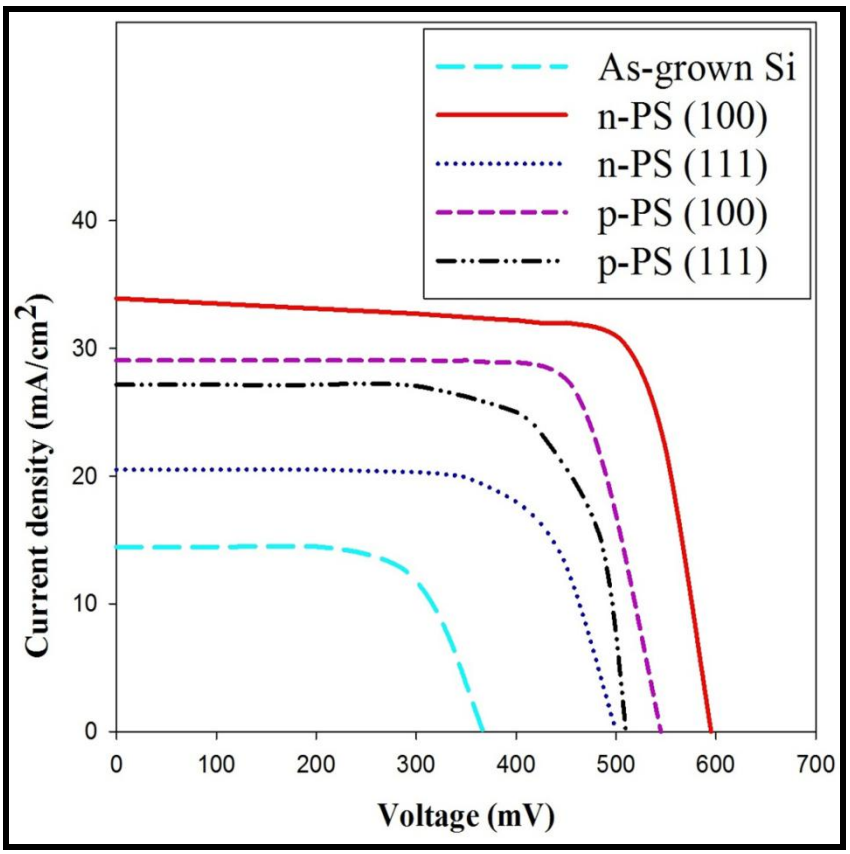

Figure 7. I-V characteristics of solar cells with PS layers formed on the n- and p-type regions with (100) and (111) orientations compared with the solar cell without a PS layer.

The results (Table 1) also show that the conversion efficiency of the solar cell with the PS ARC layer based on the n-type c-Si (100) is higher than those of the solar cells with PS ARC layers with different orientations and Si type as well as that of the solar cell without a PS ARC layer.

4. CONCLUSIONS

The effect of porosity on the morphology of the PS layers was investigated. High porosity (91%) nanopores, with an average diameter of 5.7 nm, were produced in the PS layer based on n-type c-Si (100) compared with 14.5%, 45%, and 27% for the PS layers formed on the n-type c-Si (111), p-type c-Si (100), and p-type c-Si (111) samples, respectively. The PL spectra indicated the maximum PL intensity, and the blue shift toward the lower wavelength had been observed at 639 nm (1.940 eV) because of the increase in the porosity of the PS layer based on n-type c-Si (100) and as a function of the different porosities.

The lowest effective reflectance was obtained in the PS layer based on the n-type c-Si (100), which exhibited an excellent light-trapping activity at wavelengths ranging from 400 to 1000 nm. The fabrication of solar cells based on the PS ARC layer formed on n-type c-Si (100) demonstrated that the conversion efficiency increased to 15.50%.

ACKNOWLEDGEMENTS
The authors would like to thank the research university (RU) grant, Universiti Sains Malaysia, and JUST-Jordan and TWAS-Italy Associteship for their support.

References

1. T.L. Canham, *Appl. Phys. Lett*. 57 (1990) 1046.
2. N. Koshida and H. Koyama, *Mater. Res. Soc. Symp. Proc*., 256 (1992) 219.
3. P. Vitanov, M. Kamenova, N. Tyutyundzhiev, M. Delibasheva, E. Goranova and M. Peneva, *Thin Solid Films*, 297 (1997) 299.
4. L. Santinacci, A.-M. Gonçalves, N. Simon and A. Etcheberry, *Electrochim. Acta*, 56 (2010) 878.
5. V. Lehmann, *J. Electrochem. Soc*., 140 (1993) 2836.
6. O. Bisi, S. Ossicini and L. Pavesi, *Surf. Sci. Rep*., 38 (2000) 1.
7. Y.S. Tsuo, J.R. Pitts, M.D. Landry, P. Menna, C.E. Bingham, A. Lewandowski and T.F. Ciszek, *Sol. Energy Mater. Sol. Cells*, 41-42 (1996) 41.
8. W.A. Badawy, R.M. El-Sherif and S.A. Khalil, *Electrochim. Acta*, 55 (2010) 8563.
9. W.J. Aziz, Simulation, fabrication and characterization of multilyer coated solar cells, in: School of Physics, University Science Malaysia, Penang (2011).
10. V. Torres-Costa, R. J. Martín-Palma and J. M. Martínez-Duart, *J. Appl. Phys*., 96 (2004) 4197.
11. P. Vitanov, M. Delibasheva, E. Goranova and M. Peneva, *Sol. Energy Mater. Sol. Cells*, 61 (2000) 213.
12. M. Rajabi and R. Dariani, *J. Porous Mater*., 16 (2009) 513.
13. S.-I. Na, S.-S. Kim, W.-K. Hong, J.-W. Park, J. Jo, Y.-C. Nah, T. Lee and D.-Y. Kim, *Electrochim. Acta*, 53 (2008) 2560.
14. L. Hyunwoo, E. Lee and L. Soohong, Investigation of nano-porous silicon antireflection coatings for crystalline silicon solar cells, in: Nanotechnology Materials and Devices Conference, 2006. NMDC 2006. IEEE, 2006, pp. 340-341.
15. P.L. Ossicini S. L. and Priolo F., Light emitting silicon for microphotonics, Springer-Verlag, Berlin Heidelberg (2003).
16. N. Jeyakumaran, B. Natarajan, S. Ramamurthy and V. Vasu, *IJNN*, 3 (2007) 45.
17. C. H. Chen and Y. F. Chen, *Solid State Commun*., 111 (1999) 681.
18. K. Omar, Z. Hassan, A. Ramzy and H. Abu hassan, *JOAM*, 11 (2009) 1641.
19. D.E. Aspnes, J.B. Theeten and F. Hottier, *Phys. Rev*., B 20 (1979) 3292.
20. A.Ramizy, Z. Hassan and K. Omar, *J. Mater. Sci.: Mater. Electron*., 22 (2011) 717.